ACS APPLIED MATERIALS & INTERFACES

Research Article

Cite This: ACS Appl. Mater. Interfaces 2017, 9, 40697-40706

www.acsami.org

1T-Phase Transition Metal Dichalcogenides (MoS_2, $MoSe_2$, WS_2, and WSe_2) with Fast Heterogeneous Electron Transfer: Application on Second-Generation Enzyme-Based Biosensor

Nasuha Rohaizad,[†,‡] Carmen C. Mayorga-Martinez,[†] Zdeněk Sofer,[§] and Martin Pumera*[,†]

[†]Division of Chemistry & Biological Chemistry, School of Physical and Mathematical Science and [‡]NTU Institute for Health Technologies, Interdisciplinary Graduate School, Nanyang Technological University, 637371 Singapore

[§]Department of Inorganic Chemistry, University of Chemistry and Technology Prague, CZ-166 28 Prague, Czech Republic

Supporting Information

ABSTRACT: Two-dimensional transition metal dichalcogenides (TMDs) have been in the spotlight for their intriguing properties, including a tunable band gap and fast heterogeneous electron-transfer (HET) rate. Understandably, they are especially attractive in the field of electrochemical biosensors. In this article, HET capabilities of various TMDs (MoS_2, $MoSe_2$, WS_2, and WSe_2) within group VI chemically exfoliated via *t*-BuLi intercalation are studied and these capabilities are used in the second generation electrochemical glucose biosensor. Strikingly, tungsten dichalcogenides (WS_2 and WSe_2) exhibit superior HET properties compared to that of their molybdenum counterparts (MoS_2 and $MoSe_2$). When incorporated into second generation glucose biosensors, WS_2 and WSe_2 generated a higher electrochemical responses than that of MoS_2 and $MoSe_2$, following the same trend as expected. The commendable performance by WX_2 is attributed to the dominance of 1T phase, revealed by characterization data. The developed and optimized 1T WX_2-based biosensor achieved analytical requirements of selectivity, wide linear ranges, as well as low limits of detection and quantification. The outstanding electrochemical performances of WS_2 and WSe_2 are to be recognized, adding on to the fact that they are not decorated with any metal nanoparticles. This is imperative to showcase the real potential of two-dimensional TMDs in electrochemical biosensors.

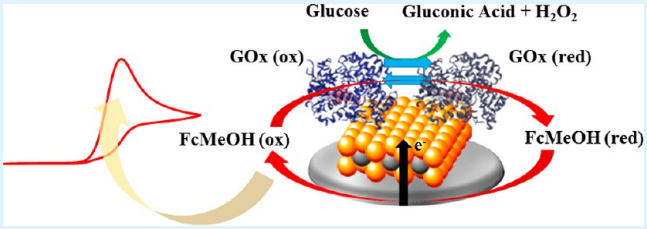

KEYWORDS: *electrochemical biosensor, second-generation glucose sensor, 2D materials, tungsten dichalcogenides, chemical exfoliation*

INTRODUCTION

The interest in two-dimensional (2D) nanomaterials resurfaced after graphene along with its striking properties was discovered in 2004.[1] Lithium intercalation exfoliation is among several other methods, namely, micromechanical exfoliation,[2,3] liquid-based direct exfoliation,[4] and chemical vapor deposition,[5−7] to prepare single or few-layered nanosheets. Owing to their size and dimensionality, a myriad of applications was realized in optoelectronics,[8] supercapacitors,[9] (bio)sensors,[10,11] as well as lubrication of interfaces.[12] Their commendable electrochemical properties, especially fast heterogeneous electron-transfer (HET) capabilities and tunable band gap, explains their dominance.[13,14] In addition, they possess lower cytotoxicity compared to that of graphene, rendering them suitable for biosensors.[15] TMDs, with such fascinating attributes, have stood out as the budding material for biosensor development towards environmental and biomedical applications.

Glucose biosensors account for approximately 85% of the current world market for biosensors due to the prevalence of diabetes in developed nations.[16] Electrochemical biosensors have been touted as a particularly promising class of analytical devices because of their exceptional performance superior to that of conventional analytical tools.[17] They offer robust and quantitative measurements by using low-cost and simple instrumentation, triggering the possibility of portability and miniaturization towards the ideal biosensor.[18] Integrating a biological recognition element prominently glucose oxidase, the electrochemical glucose biosensor, boasts a high degree of selectivity. Needless to say, there are other analytical aspects such as sensitivity, and nanomaterials have been widely studied to enhance the performance of biosensors. Recently, the exploration of 2D nanomaterials is rising in the biosensor field due to their favorable electrochemical properties.[19]

In this study, we aim to explore the potential of MoS_2 analogues towards development of a second-generation electrochemical glucose biosensor. Group VI TMDs, $MoSe_2$, WS_2, and WSe_2, together with MoS_2 are materials of interest prepared by *t*-BuLi intercalation and exfoliation. Their intriguing HET capabilities will be compared, and the superior pure TMD(s) is further developed into a biosensor without any doping or decoration with nanoparticles of noble metals.

Received: August 29, 2017
Accepted: October 16, 2017
Published: November 7, 2017

DOI: 10.1021/acsami.7b13090
ACS Appl. Mater. Interfaces 2017, 9, 40697−40706

Scheme 1. Schematic Representation Illustrating (a) Exfoliation of Bulk TMDs Employing *t*-BuLi as the Intercalating Agent; (b) Construction of the Biosensor Electrode by Drop Casting Exfoliated TMDs onto Bare GC electrode, Followed by (c) GOx, Then (d) Cross-Linking Using GTA; Finally, (e) Electrochemical Detection Mechanism of Glucose

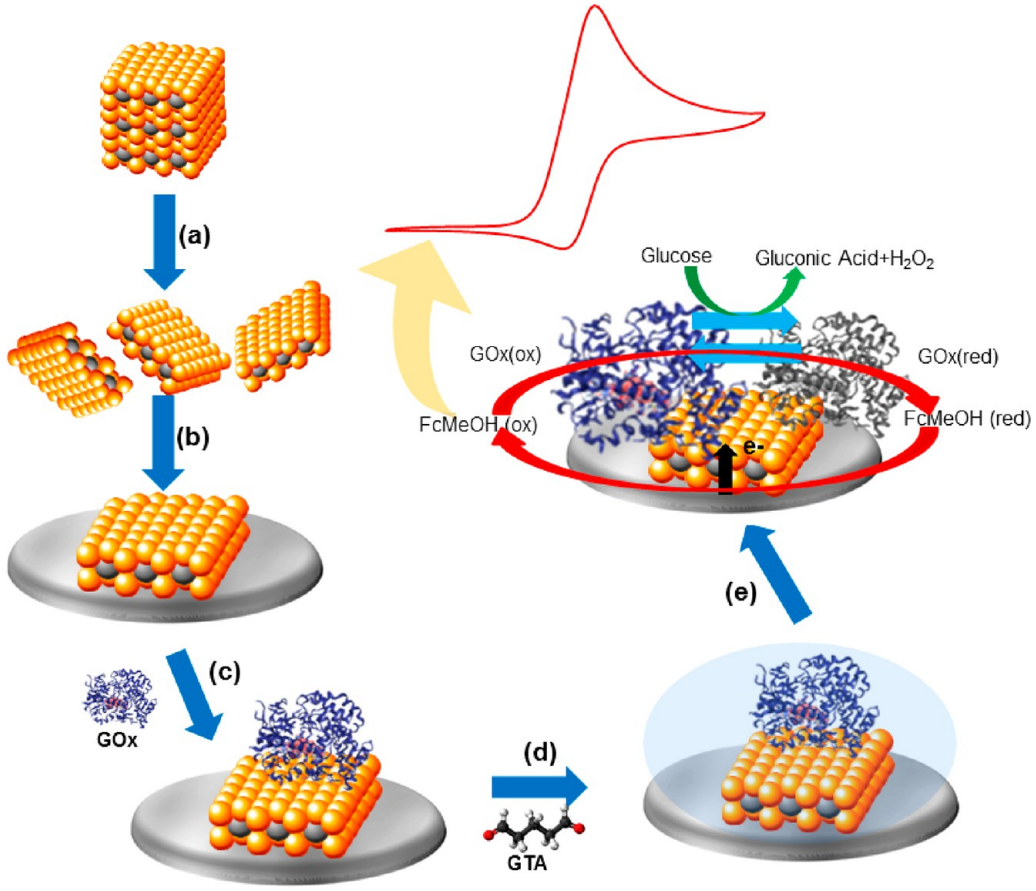

RESULTS AND DISCUSSION

In this work, we investigate the heterogeneous electron-transfer (HET) rate of group VI TMDs (MoS_2, $MoSe_2$, WS_2, and WSe_2) chemically exfoliated using *tert*-butyllithium (*t*-BuLi) organic intercalant towards developing a second-generation electrochemical glucose biosensor. Once the materials were prepared, various characterization methods, including transmission electron microscopy (TEM) and X-ray photoelectron spectroscopy (XPS), were performed to elucidate the structure of the exfoliated compounds along with their properties. These TMDs were then incorporated into the biosensor by drop casting onto a bare glassy carbon (GC) electrode, followed by glucose oxidase (GOx) and then glutaraldehyde (GTA). Their performances in detecting glucose were compared via oxidation signals of ferrocenemethanol (FcMeOH), the mediator (Scheme 1). Analytical parameters of the glucose biosensor based on the superior performing TMD(s) were established thereafter.

The four group VI TMDs were foremost characterized consequent to their preparation by *t*-BuLi intercalation and exfoliation. TEM images display individual few-layer sheets with sizes up to a micron, also reflecting the varying extents of exfoliation of the materials (Figure 1A–D). High-resolution TEM (HR-TEM) and selective area electron diffraction (SAED) were additionally carried out to shed light on the atomic arrangement. Both honeycomb and hexagonal lattices are observed, implying that both 2H and 1T phases are present accordingly (Figure 1E–H).[20]

The existence of the 1T phase is a prominent feature of the lithium intercalation method, where phase transformation occurs.[21] The electron donating nature of lithium induces an effective change in the d electron count of the host consequently destabilizing the naturally occurring 2H phase to form 1T phase.[22,23] The crystal symmetry and electronic structures differ across phases along with their properties.[24] The 2H phase has a hexagonal symmetry, with a trigonal prismatic metal coordination, as the layers of chalcogen atoms are stacked directly above one another. In contrast, the 1T phase has a tetragonal symmetry, with an octahedral metal coordination, as the layers are offset from each other. The conductivity of 2H is semiconducting, whereas 1T is metallic, in which the latter is recognized for its reactivity towards functionalization[25,26] as well as enhancing electrochemical properties.[27] Moreover, both edge and basal sites are active in 1T-phase TMDs, further improving the electrocatalytic performance.[28,29] With good conductivity, fast electron-transfer kinetics, and increased catalytic sites, these 1T-TMDs are anticipated to promote the signal transduction of an electrochemical biosensor.

Figure 2 shows the X-ray diffraction (XRD) data, shedding light on the extent of exfoliation and phase purity. A pronounced (00*l*) diffraction peak is observed for all exfoliated TMDs, implying a well-ordered stacking structure composed of few layers.[30] With an exception of $MoSe_2$, the materials prepared are pure along with a high preferential orientation. The diffractogram of $MoSe_2$, on the contrary, reveals peaks corresponding to other

DOI: 10.1021/acsami.7b13090
ACS Appl. Mater. Interfaces 2017, 9, 40697–40706

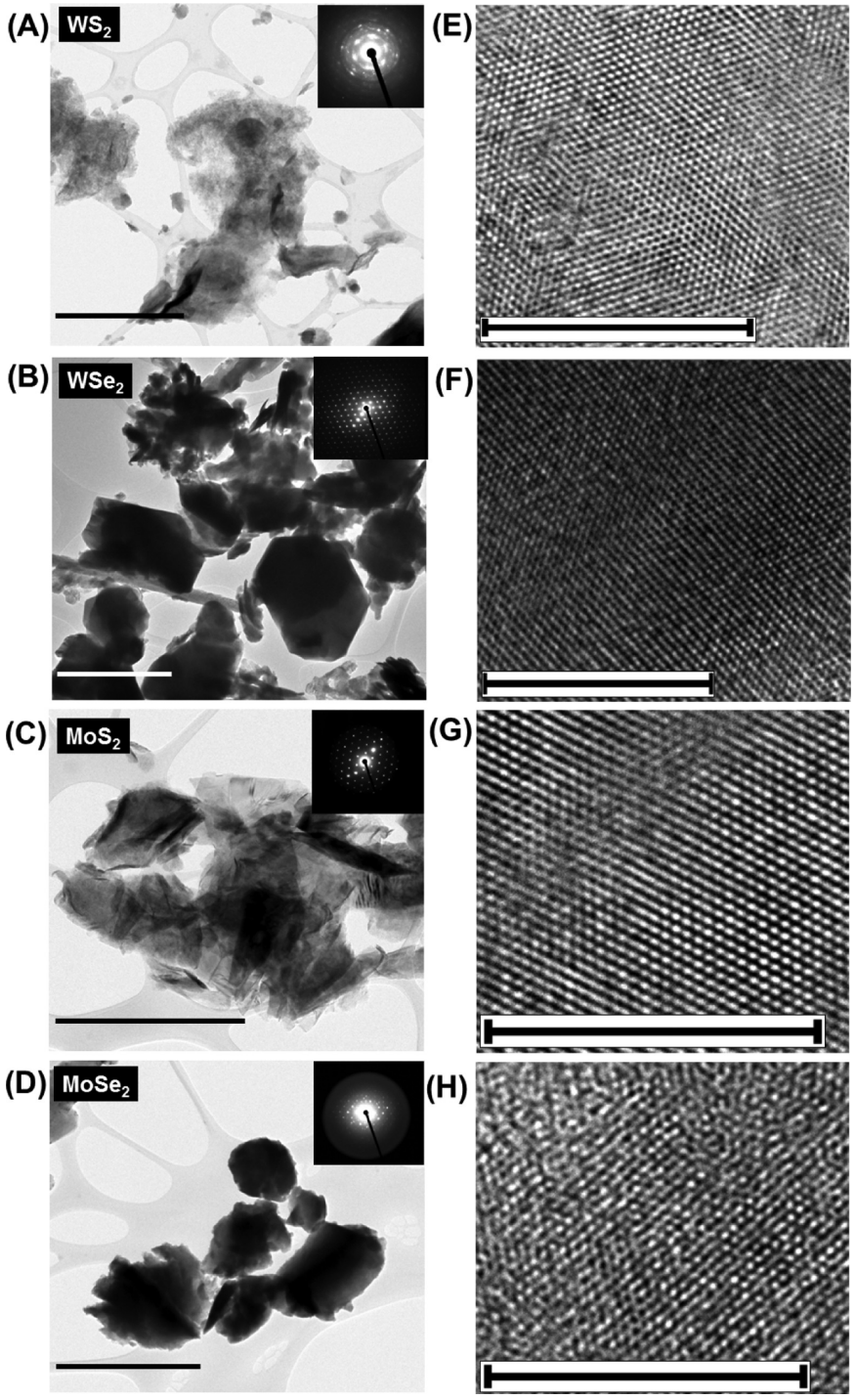

Figure 1. TEM micrographs with SAED (inset) (A–D) and HR-TEM (E–H) of the *t*-BuLi-based exfoliated WS_2, WSe_2, MoS_2, and $MoSe_2$, respectively. Scale bar: TEM = 1 μm and HR-TEM = 10 nm.

crystal planes.[31,32] They can be assigned to the semiconducting 2H, highlighting the significant phase existence in $MoSe_2$.

Upon characterization of the exfoliated 2D TMDs and realization of their metallic and crystalline nature, the electrochemical performances of these materials were studied prior to the development of an electrochemical glucose biosensor. A study of their heterogeneous electron-transfer (HET) capabilities was conducted by employing ferro/ferricyanide, a redox probe sensitive toward the surface of electrode materials.[33] The HET rate is an imperative electrocatalytic parameter correlated to peak-to-peak separation (ΔE_p), where a narrow separation between anodic and cathodic peaks translates to a fast HET rate.[34] ΔE_p of the four materials was attained and ranked in the ascending order: WSe_2 < WS_2 < $MoSe_2$ < MoS_2 < GC electrode (Figure 3A). With the smallest ΔE_p, WSe_2 exhibits the fastest HET rate and therefore offers the best electrocatalytic performance for sensing applications.

As FcMeOH is involved as the mediator to second-generation biosensors, HET capabilities of the materials were compared in an electrolyte consisting of FcMeOH dissolved in PBS. A slight deviation from the previous results was obtained on the basis of ΔE_p: WSe_2, GC electrode < WS_2 < $MoSe_2$ < MoS_2 (Figure 3B).

DOI: 10.1021/acsami.7b13090
ACS Appl. Mater. Interfaces 2017, 9, 40697–40706

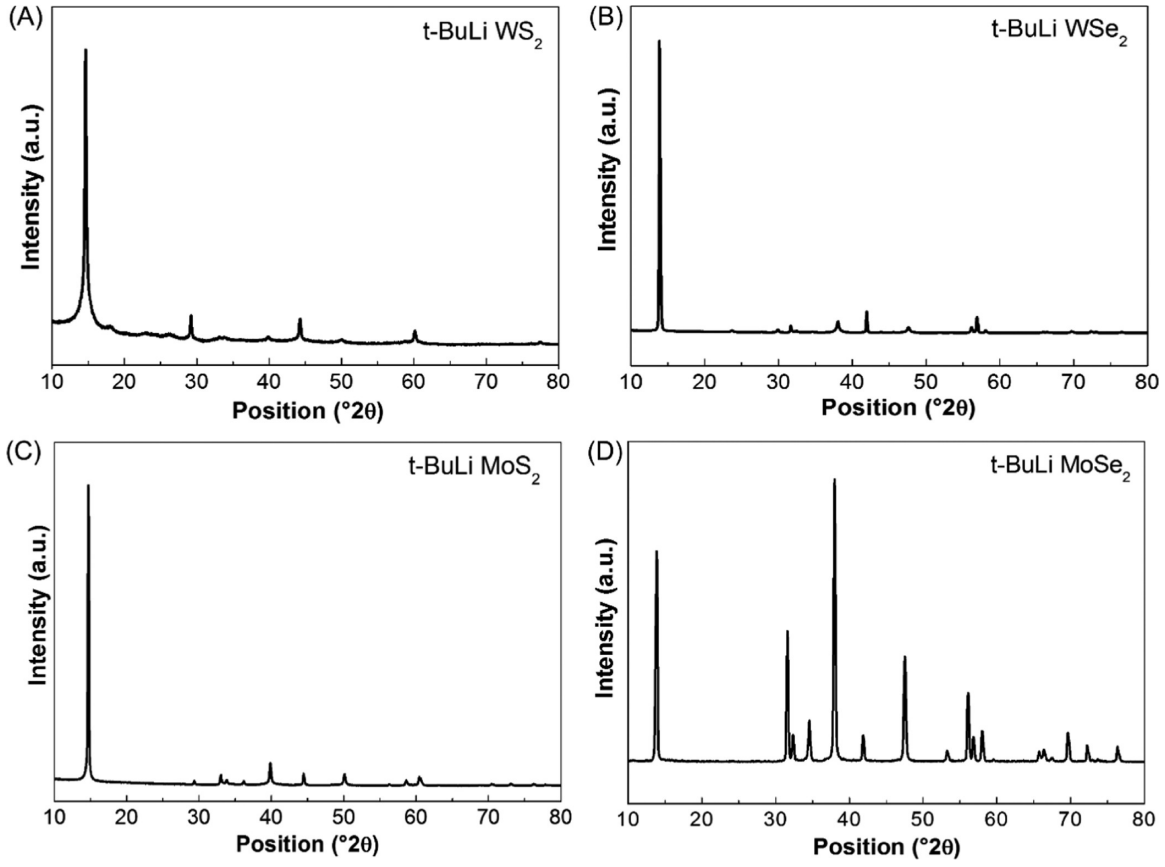

Figure 2. X-ray diffraction (XRD) of (A) WS_2, (B) WSe_2, (C) MoS_2, and (D) $MoSe_2$ *t*-BuLi-exfoliated TMDs.

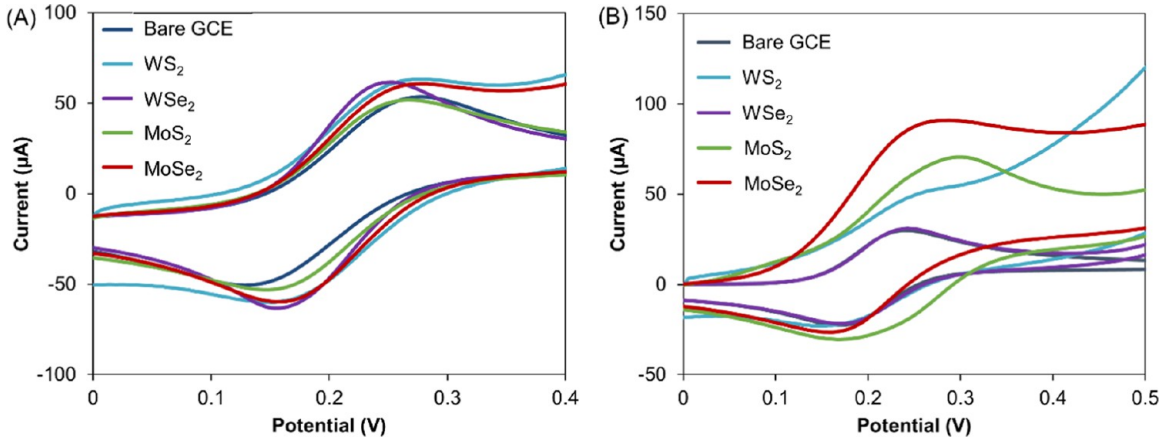

Figure 3. Cyclic voltammograms of the four prepared TMDs against bare GC electrode in (A) 5 mM $[Fe(CN)_6]^{4-/3-}$ in 0.1 M KCl and (B) 2 mM FcMeOH in phosphate-buffered saline (PBS) (pH 7.2) for HET studies. Conditions: scan rate, 100 mV s^{-1}.

Nonetheless, the tungsten dichalcogenides outperformed their molybdenum counterparts with WSe_2 again demonstrating the best HET capability.

After we determined the HET capabilities, the second-generation glucose oxidase (GOx)/*t*-BuLi-based TMD glucose biosensor is implemented and evaluated. Figure 4 presents the cyclic voltammograms of the biosensor in 2 mM FcMeOH in PBS (pH 7.2) and in the presence of 10 or 0.5 mM of glucose accordingly. The disparity in the glucose detection response is apparent among the materials.

Comparing the performance of the glucose biosensor as a function of the TMDs, both WS_2 and WSe_2 similarly generated the highest response, followed by MoS_2 and then $MoSe_2$. The superior performance of WX_2 (X = S, Se) is attributed to their significant metallic 1T phase, the phase responsible for the commendable electrocatalytic activity. This is substantiated by XPS, which reveals their surface elemental composition. Zooming in to the high-resolution W 4f spectra (Figure 5), peaks corresponding to W $4f_{7/2}$ and W $4f_{5/2}$ are observed. Further deconvolution of both metal and chalcogen spectra provides the phase composition, 2H and 1T,[28] in which the latter is dominant. Cross-referencing to relevant XPS data in the literature, the metallic phase of WX_2 is higher in composition than that of MoX_2 for both X = S, Se.[35]

DOI: 10.1021/acsami.7b13090
ACS Appl. Mater. Interfaces 2017, 9, 40697−40706

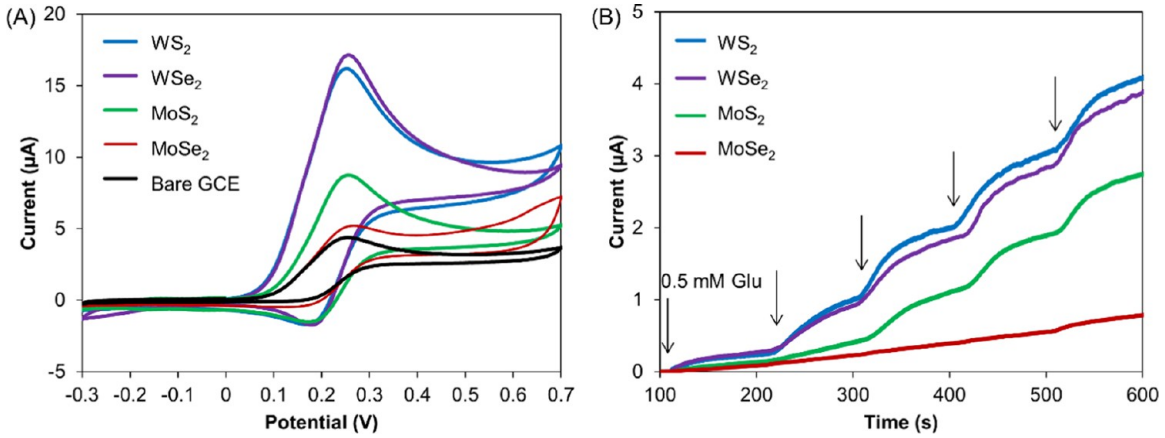

Figure 4. (A) Cyclic voltammogram (10 mM glucose; scan rate, 100 mV s^{-1}) and (B) chronoamperometry data (0.5 mM glucose added every 100 s; potential, 0.1 V) of the second-generation electrochemical glucose biosensor based on different 1T-TMDs. Conditions: electrolyte, FcMeOH (2 mM) in PBS (pH 7.2).

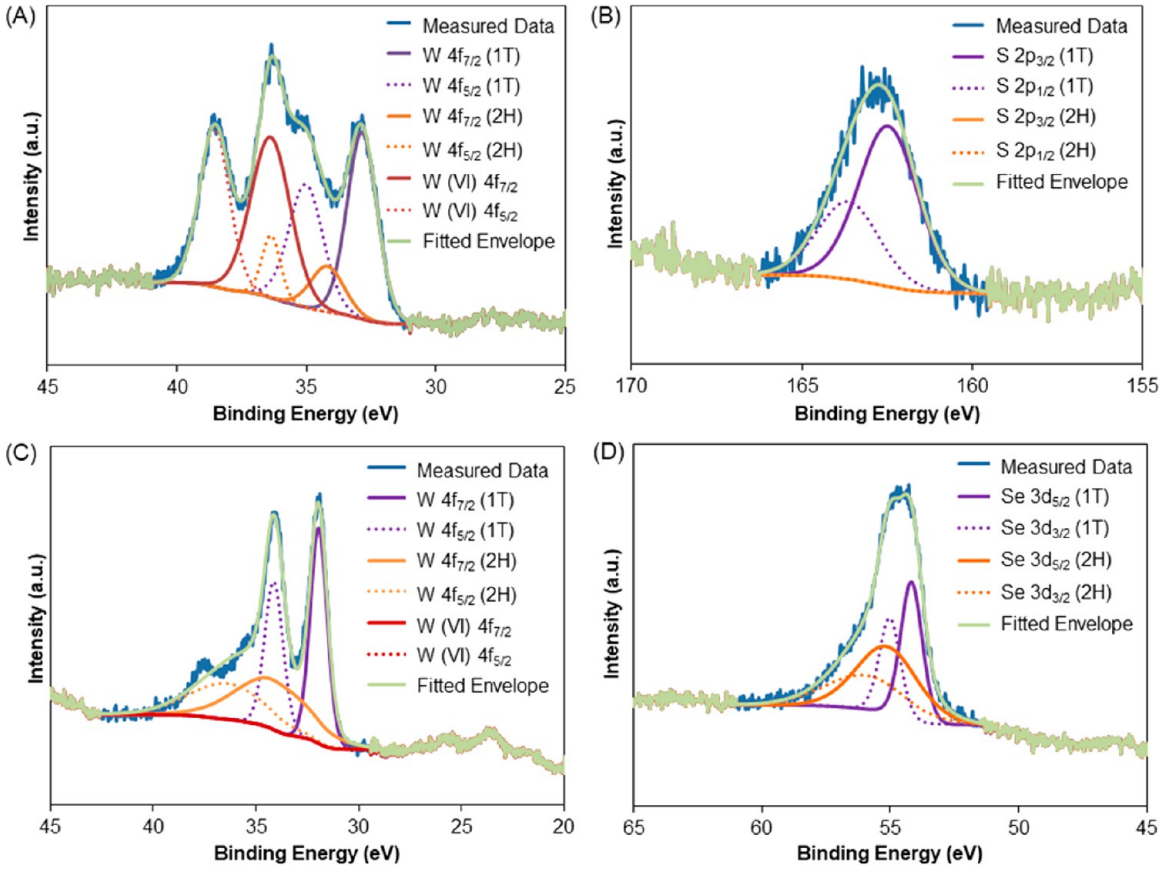

Figure 5. High-resolution X-ray photoelectron spectra of (A) W 4f and (B) S 2p regions of 1T-WS_2, (C) W 4f, and (D) Se 3d regions of 1T-WSe_2.

One factor which influences the higher proportion of metallic 1T phase in WX_2 (X = S, Se) is the extent of exfoliation, which depends on the metal/chalcogen composition and intercalating agent.[36] Apparent in $MoSe_2$, earlier characterization data presented in this article shows the poor exfoliation of the material. The phase transformation to 1T could be inefficient, therefore lacking in metallicity to promote the biosensor's performance. Another plausible contributing factor is the stability of the metallic 1T phase. It is to be put forth that 1T-WS_2 is more stable than MoS_2[20,37] based on the transition temperatures and activation barrier for the 1T to 2H restoration.[38,39] Our results suggest that the comparison could extend beyond sulfides and be applied to selenides as well.

Energy dispersive X-ray spectroscopy (EDS) may also provide an explanation for the electrochemical performances. Apart from verifying the elemental composition of the materials, the elemental atomic percentages are acquired (Figure S1 in the Supporting Information). The metal/chalcogen ratio (M/X) of WX_2 is closer or even exceeding 2, the ideal theoretical value for TMDs, unlike MoX_2. Henceforth, the M/X ratio possibly influences electrochemical properties.

DOI: 10.1021/acsami.7b13090
ACS Appl. Mater. Interfaces 2017, 9, 40697−40706

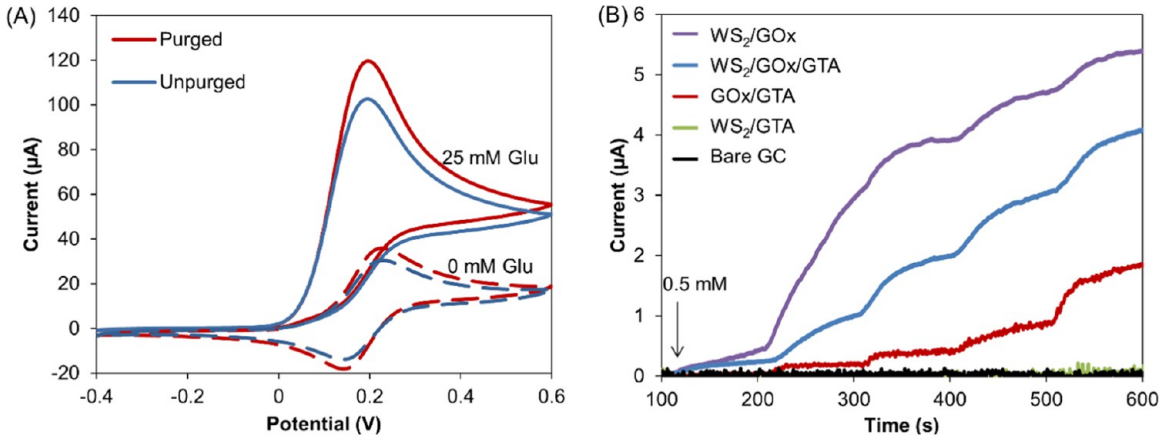

Figure 6. (A) Cyclic voltammogram comparing responses of a WS_2-based biosensor in N_2 purged against unpurged conditions (25 mM glucose, scan rate, 100 mV s^{-1}) and (B) chronoamperometry data (0.5 mM glucose added every 100 s; potential, 0.1 V) of a second-generation electrochemical glucose biosensor based on different electrode configurations. Conditions: electrolyte, FcMeOH (2 mM) in PBS (pH 7.2).

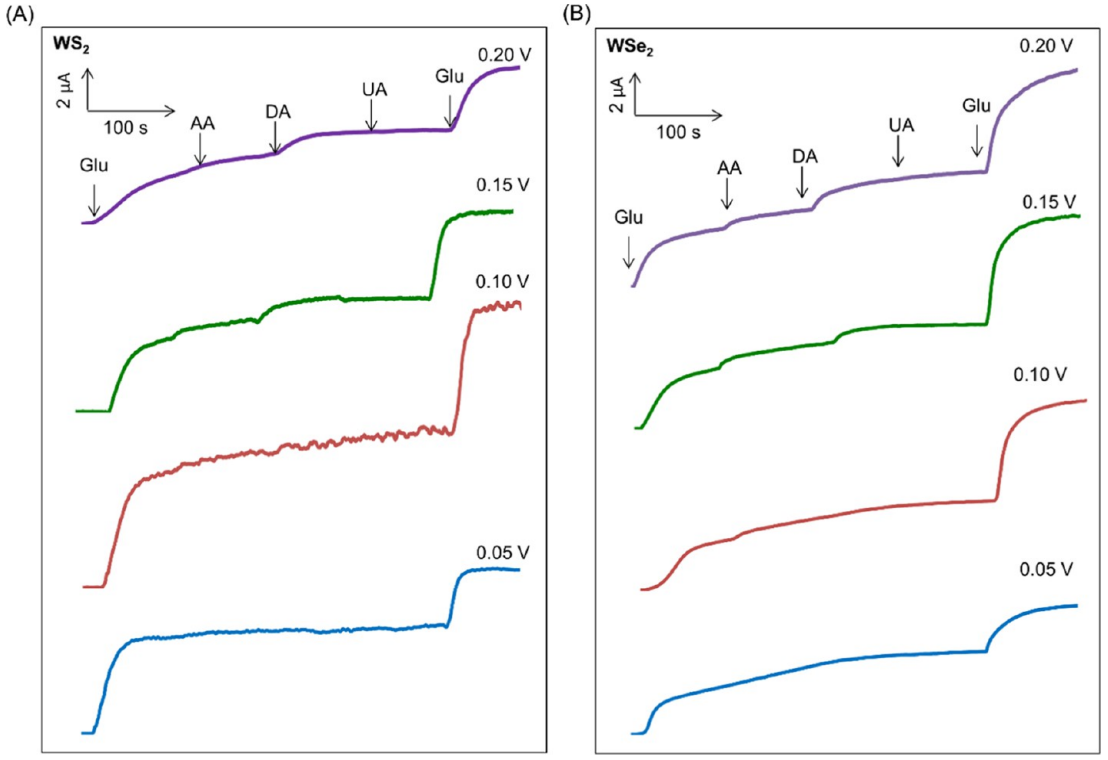

Figure 7. Chronoamperometry data of both WX_2-biosensors, (A) WS_2 and (B) WSe_2, for interference studies. Glucose (5 mM), L-ascorbic acid (0.2 mM), dopamine hydrochloride (0.2 mM), uric acid (0.2 mM), and glucose (5 mM) were added sequentially every 100 s at varying potentials. Conditions: electrolyte, FcMeOH (2 mM) in pH 7.2 PBS.

Overall, the various characterization techniques, such as XRD, XPS, and EDS, substantiate the superior electrochemical performance and HET capabilities of WS_2 and WSe_2. The dominance of 1T phase, together with a satisfactory metal/chalcogen ratio, are important attributes to possess, especially in the context of biosensors. Subsequently, the glucose biosensors are developed on the basis of these two tungsten dichalcogenides.

The detection mechanism of glucose in this second-generation biosensor (Scheme 1e) begins with an enzymatic breakdown, particularly at the flavin redox center (FAD) of GOx (eq 1). Instead of relying on O_2 as the cofactor to regenerate FAD-GOx, FcMeOH intervenes as the mediator (eq 2). The electron transfer to the electrode surface is made more efficient as FcMeOH is small enough to access the deeply buried flavin redox center.[40,41] Interconversion between ferrocene (FcMeOH) and ferrocenium ion (Fc^+MeOH) eventually gives rise to an oxidation signal that correlates to glucose levels (eq 3).[42] This signal is achieved more efficiently and at a lower potential due to the presence of TMDs.

$$\text{glucose} + \text{FAD-GOx} + 1/2\ O_2 \rightarrow \text{gluconic acid} + \text{FADH}_2\text{-GOx} + H_2O_2 \quad (1)$$

$$\text{FADH}_2\text{-GOx} + 2\ Fc^+\text{MeOH} \rightarrow \text{FAD-GOx} + 2\ \text{FcMeOH} + 2\ H^+ \quad (2)$$

DOI: 10.1021/acsami.7b13090
ACS Appl. Mater. Interfaces 2017, 9, 40697−40706

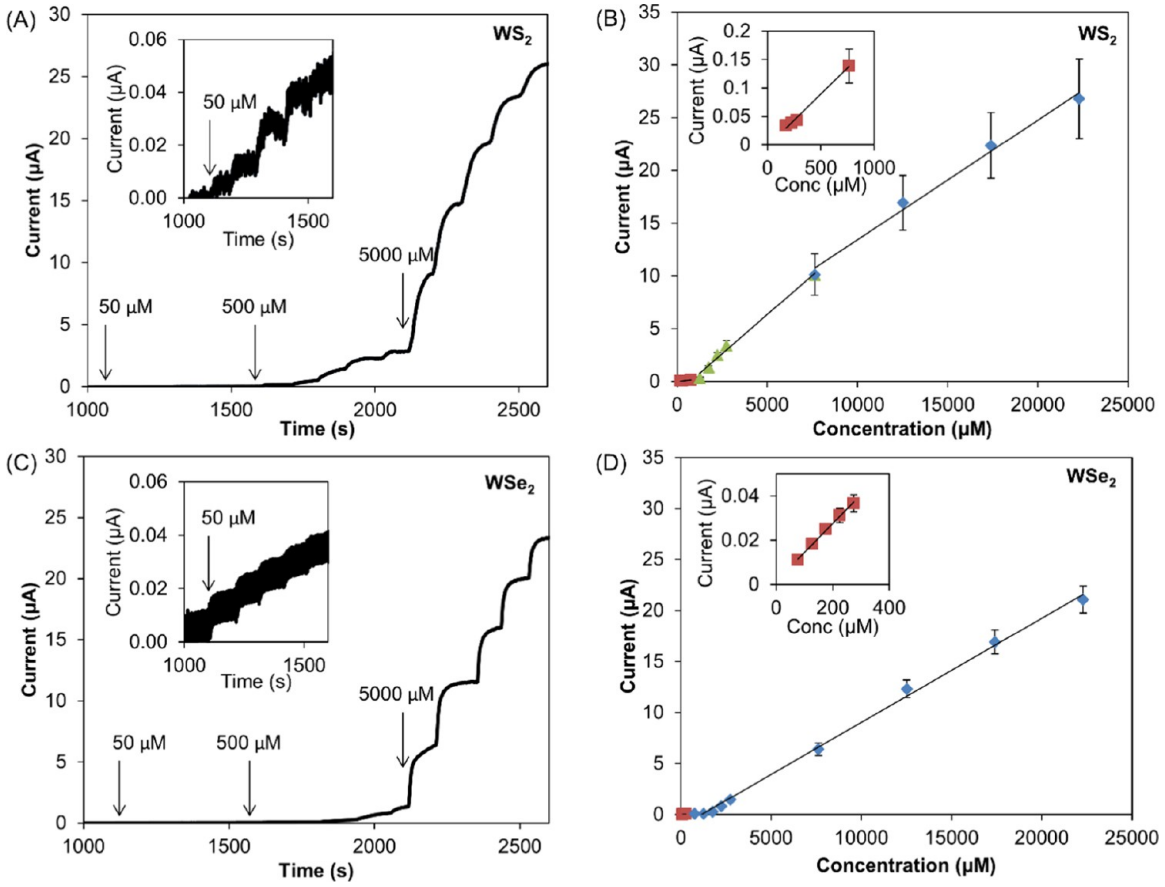

Figure 8. Chronoamperometry data and calibration plots for WS_2 (A, B)- and WSe_2 (C, D)-based electrochemical glucose biosensors. Conditions: electrolyte, FcMeOH (2 mM) in pH 7.2 PBS; potential, 0.1 V.

$$2\ \mathrm{FcMeOH} \xrightarrow[100\ \mathrm{mV}]{\mathrm{TMDs}} 2\ \mathrm{Fc^{+}MeOH} + 2\ \mathrm{e^{-}} \quad (3)$$

The mechanism of the glucose biosensor is confirmed on the basis of WS_2 as the model. Two assays were performed, one in N_2-purged FcMeOH/PBS buffer solution, whereas the other in unpurged condition (Figure 6A). The same trend is observed for both conditions, where anodic current signals increase significantly in the presence of glucose. This confirms the detection mechanism for the developed biosensor. However, the current signals are slightly lower in unpurged solution, indicating a possible competition with oxygen to regenerate the oxidized form of the redox center of GOx. The signal is nonetheless from the oxidation of FcMeOH ion, performing its part as a mediator.

Supplementarily, each biosensor component is scrutinized to understand and affirm their roles (Figure 6B). GOx is critical as the biorecognition element of glucose which triggers the detection mechanism (red curve), whereas WS_2 enhances the signal that arises from the oxidation of FcMeOH ion (purple curve). GTA is necessary to stabilize the biosensor as GOx is immobilized via cross-linking (blue curve). The performance of the biosensor, however, is compromised as the layer may hinder the shuttling of electrons between the active site of enzyme and the mediator. In absence of the GOx, no response is recorded (green and black curves).

Moving on to optimize the electrochemical glucose biosensor, the concentration of 1T WX_2 drop casted onto bare GC electrode was varied. A 5.0 mg/mL suspension in water produces the best results (Figure S2, Supporting Information). A lower concentration implies lesser amount of the catalytic material for enhancing the signal, whereas too high a concentration of TMDs on the electrode surface may block the signal transduction.

Another aspect optimized was the operating potential based on selectivity to fulfill an analytical criterion of any developed biosensor. There are endogenous compounds present in blood at concentrations 30 times lower than that of glucose,[43] such as L-ascorbic acid (AA), dopamine hydrochloride (DA), and uric acid (UA). They pose as interferences to the measurements because they are electrochemically active. To preferentially detect the analyte of interest, the operating potential could simply be tuned. This was carried out while adding physiological levels of glucose (5 mM) and interferences (0.2 mM). For both WS_2 and WSe_2, low potentials of 0.10 and 0.05 V successfully eliminate contributions from the aforementioned compounds. The operating potential is ultimately set at 0.10 V, as the intensity of the desired signal is not compromised (Figure 7).

After we determine the optimum working potential where the interferences species do not affect the biosensors' response, the calibration curves were performed for both biosensor WX_2 materials. The WS_2-based biosensor detects glucose in three linear ranges (Figure 8A, B), 176−766 μM (r = 0.997), 1.3−7.7 mM (r = 0.996), and 7.7−22.3 mM (r = 0.995), whereas the WSe_2-based biosensor in two (Figure 8C, D), 77−274 μM (r = 0.999) and 0.77−22.3 mM (r = 0.998). Meanwhile, the limit of detection (LOD) and limit of quantification (LOQ) are calculated according to the IUPAC approach.[44] Representing the lowest concentration of analyte that can be reliably measured by an analytical procedure, LOD and LOQ were, respectively,

DOI: 10.1021/acsami.7b13090
ACS Appl. Mater. Interfaces 2017, 9, 40697−40706

Table 1. Comparison of TMD-Based Electrochemical Glucose Biosensors

electrode platform	transduction method	generation of biosensor	linear range	detection limit (μM)	ref
GCE/WS_2/GOx/GTA	chronoamperometry	second gen	180−770 μM 1.3−7.6 mM 7.6−22.3 mM	82.6	this work
GCE/WSe_2/GOx/GTA	chronoamperometry	second gen	77−274 μM 0.77−22.3 mM	52.0	
GCE/APTES/chitosan/rMoS_2/GOx	voltammetry	first gen	3−20 mM		48
GCE/AuNPs@MoS_2-GOx/Nafion	voltammetry	first gen	10−300 μM	2.8	49
Au/AuNPs-MoS_2/GOx	chronoamperometry	second gen	0.25−13.2 mM	0.042	50

computed to 82.6 and 275 μM for WS_2 and 52.0 and 173 μM for WSe_2.

In terms of analytical aspects, the WSe_2-based biosensor performed better. Two linear ranges were attained, the second one covering a wide spectrum of concentrations. Furthermore, the LOD and LOQ are lower compared to those of WS_2. This is justified by the HET rate, where WSe_2 gave rise to narrow ΔE_p, implying better capability for electrochemical sensing of glucose. Another notable observation is the other peak corresponding to W (VI) in XPS data. This is contributed by the oxidized species WO_3 that may be formed during sample preparation and transfer.[45] The oxidized peak is significantly prominent in WS_2 than WSe_2, in agreement with another report,[46] influencing their electrochemical performances.

Finally, the feasibility of the developed WSe_2-based electrochemical glucose biosensor was tested with a real sample. The human serum from Sigma-Aldrich was used as received. Already comprising of 3.33−7.78 mM glucose,[47] the sample is introduced into the electrolyte solution, then generating a response. The concentrations were extrapolated from the calibration graph and obtained to be 2.36 ± 0.78 mM for WSe_2 (n = 3). The values are close to the lower value of the range stipulated.

Other TMD-based electrochemical glucose biosensors in the literature developed based on MoS_2 were either pretreated or decorated with Au nanoparticles (Table 1). Some of the linear ranges either fall much lower than the physiological levels or in the upper limits. In our case, we report a second-generation glucose biosensor based solely on 1T-phase WS_2 and WSe_2. The developed biosensors have linear ranges for different orders of concentration and relatively low LOD, offering flexibility in future developments of electrochemical biosensors for biomedical and environmental applications.

CONCLUSIONS

We herein put forth the superior electrochemical properties of tungsten dichalcogenides (WS_2, WSe_2) over their molybdenum counterparts (MoS_2, $MoSe_2$) in the context of a second-generation electrochemical glucose biosensor. These four group VI TMDs were prepared via *t*-BuLi intercalation and exfoliation prior to a comparison of their electrochemical performance, particularly HET capabilities. With narrower separation between anodic and cathodic peaks in redox probes, both WS_2 and WSe_2 demonstrate a faster HET rate. Characterization data revealed the prominence of metallic 1T phase, a polymorph affirmed to improve electrocatalytic properties. The outstanding electrochemical performance then motivated the incorporation of 1T-phase WX_2 into a second-generation glucose biosensor. Analytical parameters were commendably achieved without any pretreatment or functionalization of noble metals, unlike the TMD-based electrochemical glucose biosensor in the literature.

EXPERIMENTAL SECTION

Chemicals. Tungsten sulfide (99.8%), tungsten selenide (99.8%), molybdenum (IV) sulfide (99.9%), and molybdenum (IV) selenide (99.9%) were acquired from Alfa Aesar, Germany. *tert*-Butyllithium (1.7 M in pentane) was acquired from Sigma-Aldrich, Czech Republic. Hexane was acquired from Lach-ner, Czech Republic. Argon (99.9999% purity) was acquired from SIAD, Czech Republic. Phosphate-buffered saline (pH 7.2) was prepared with potassium chloride (max 0.0001% Al), potassium dihydrogen phosphate, and sodium hydrogen phosphate; these three chemicals were acquired from Sigma-Aldrich, Singapore. Potassium hexacyanoferrate (II) trihydrate (≥98.5%), potassium hexacyanoferrate (III) (~99%), glucose oxidase from *Aspergillus niger* (EC 1.1.3.4, type X-S), glutaraldehyde solution (50% in water), D-(+)-glucose (≥99.5%), L-ascorbic acid (BioXtra, ≥99.0%, crystalline), uric acid (≥99%, crystalline), and dopamine hydrochloride were also acquired from Sigma-Aldrich, Singapore. Ferrocenemethanol (>95%) was acquired from Tokyo Chemical Industry.

Instrumentation. Electrochemical measurements, both voltammetric and chronoamperometric, were performed with a μAutolab type III electrochemical analyzer (Eco Chemie, The Netherlands) connected to a personal computer and controlled by the software, NOVA version 1.10. Measurements were carried out at room temperature using a three-electrode system in a glass cell: a glassy carbon working electrode (3 mm diameter) modified with the material of interest and other components, platinum auxiliary electrode, as well as Ag/AgCl reference electrode. Scanning electron microscopy and energy dispersive X-ray spectroscopy (EDS) were carried out using a Jeol 7600F instrument (Jeol, Japan) operating at acceleration voltage of 5 and 15 kV, respectively. X-ray photoelectron spectroscopy (XPS) measurements were carried out using a Phoibos 100 spectrometer and a monochromatic Mg X-ray radiation source (SPECS, Germany). XPS data was consequently processed with Casa XPS, where the relative sensitivity factor, area constraint, and position constraint were set to obtain a good fitting. The sample preparation for the aforementioned characterization techniques involved grinding TMDs in a solid form using a mortar, then placing as a uniform layer onto a carbon-conductive tape. High-resolution transmission electron microscopy (HR-TEM) data were obtained with the EFTEM Jeol 2200 FS microscope (Jeol, Japan), operating at an acceleration voltage of 200 keV. The sample preparation involved drop casting of the suspension (1 mg mL^{-1} in water) on a TEM grid (Cu; 200 mesh; Formvar/carbon), then drying at 60 °C for 12 h. X-ray diffraction (XRD) was performed using a Bruker D8 Discoverer powder diffractometer with parafocusing Bragg−Brentano geometry and Cu Kα radiation (λ = 0.15418 nm, U = 40 kV, I = 40 mA). Data were collected at room temperature over an angular range of 10−80° (2θ), with a step size of 0.02° (2θ). The EVA software was used to evaluate the results.

Exfoliation of Bulk Materials. The bulk materials (WS_2, WSe_2, MoS_2, and $MoSe_2$) were exfoliated in close accordance to reported protocols.[51,52] Each of their TMD powder was first added to 20 mL of *tert*-butyllithium (*t*-BuLi) in pentane (1.7 M), obtaining four different suspensions. They were then stirred at 25 °C under argon atmosphere for 72 h. The desired Li-intercalated materials were separated by suction filtration under argon atmosphere and washed repeatedly with hexane (dried over Na). Hundred milliliters of water was subsequently added and centrifugation (18 000g) was performed repeatedly until the

DOI: 10.1021/acsami.7b13090
ACS Appl. Mater. Interfaces 2017, 9, 40697−40706

conductivity fell below 20 μS. Finally, they were dried in a vacuum oven at 25 °C for 48 h, yielding *t*-BuLi-exfoliated TMDs.

Biosensor Preparation. Suspensions of *t*-BuLi-exfoliated TMDs were prepared by dispersing the respective materials in ultrapure water (5 mg mL^{-1}). Ultrasonication was carried out for 3 h to ensure a homogenous and well-dispersed suspension. For subsequent usage, the suspension would be ultrasonicated for 5 min. The GCE electrodes were polished with 0.05 μm alumina powder on a polishing pad, rinsed with ultrapure water, and blown dry with N_2 gas. The modification of electrodes first involved drop casting 3 μL of *t*-BuLi-exfoliated TMD suspension, then left to dry in ambient conditions. Once dried, 5 μL of glucose oxidase in ultrapure water (0.1 g mL^{-1}, GOx) was drop casted and similarly left to dry in ambient conditions. Five microliters of glutaraldehyde in ultrapure water (0.25%, GTA) was drop casted last and dried in the oven at 35 °C for 30 min. As such, a TMD/GOx/GTA-modified electrode was prepared and would be stored in the refrigerator at 4 °C when not in use.

Electrochemical Measurements. Heterogeneous electron-transfer (HET) studies were carried out using cyclic voltammetry (CV) between the potentials of −0.3 and 0.7 V, at a scan rate of 100 mV s^{-1}. The redox probe potassium hexacyanoferrate (5 mM) was prepared in supporting electrolyte potassium chloride (0.1 M). Other CV measurements were carried out in ferrocenemethanol (FcMeOH, 2 mM) in phosphate-buffered saline solution (PBS, pH 7.2). Specific concentrations of glucose were injected into the electrolyte and stirred for 2 min before each measurement, performed between −0.4 and 0.6 V at a scan rate of 100 mV s^{-1}. Meanwhile, chronoamperometry ($\Delta t > 1$ ms) was performed at a fixed constant potential of 0.1 V. Specific concentrations of glucose were injected into the solution every 100 s, where stirring was continuous throughout the measurement. The acquired data was subjected to smoothing and baseline correction for further analysis.

■ ASSOCIATED CONTENT

Supporting Information

The Supporting Information is available free of charge on the ACS Publications website at DOI: 10.1021/acsami.7b13090.

EDS of the four *t*-BuLi-based exfoliated TMDs; chronoamperometry data optimizing drop cast concentration of WX_2 (PDF)

■ AUTHOR INFORMATION

Corresponding Author

*E-mail: pumera.research@gmail.com.

ORCID

Zdeněk Sofer: 0000-0002-1391-4448

Martin Pumera: 0000-0001-5846-2951

Notes

The authors declare no competing financial interest.

■ ACKNOWLEDGMENTS

M.P. acknowledges a Tier 1 grant (99/13) from the Ministry of Education, Singapore. Z.S. was supported by Czech Science Foundation (GACR No. 16-05167S). This work was created with the financial support of the Neuron Foundation for science support. This work was supported by the project Advanced Functional Nanorobots (reg. No. CZ.02.1.01/0.0/0.0/15_003/0000444 financed by the EFRR).

■ REFERENCES

(1) Novoselov, K. S.; Geim, A. K.; Morozov, S. V.; Jiang, D.; Zhang, Y.; Dubonos, S. V.; Grigorieva, I. V.; Firsov, A. A. Electric Field Effect in Atomically Thin Carbon Films. *Science* **2004**, *306*, 666−669.

(2) Lee, C.; Yan, H.; Brus, L. E.; Heinz, T. F.; Hone, J.; Ryu, S. Anomalous Lattice Vibrations of Single- and Few-Layer MoS_2. *ACS Nano* **2010**, *4*, 2695−2700.

(3) Li, H.; Lu, G.; Wang, Y.; Yin, Z.; Cong, C.; He, Q.; Wang, L.; Ding, F.; Yu, T.; Zhang, H. Mechanical Exfoliation and Characterization of Single- and Few-Layer Nanosheets of WSe_2, TaS_2, and $TaSe_2$. *Small* **2013**, *9*, 1974−1981.

(4) Niu, L.; Coleman, J. N.; Zhang, H.; Shin, H.; Chhowalla, M.; Zheng, Z. Production of Two-Dimensional Nanomaterials via Liquid-Based Direct Exfoliation. *Small* **2016**, *12*, 272−293.

(5) Li, S.; Wang, S.; Tang, D.-M.; Zhao, W.; Xu, H.; Chu, L.; Bando, Y.; Golberg, D.; Eda, G. Halide-Assisted Atmospheric Pressure Growth of Large WSe_2 and WS_2 Monolayer Crystals. *Appl. Mater. Today* **2015**, *1*, 60−66.

(6) Reale, F.; Sharda, K.; Mattevi, C. From Bulk Crystals to Atomically Thin Layers of Group VI- Transition Metal Dichalcogenides Vapour Phase Synthesis. *Appl. Mater. Today* **2016**, *3*, 11−22.

(7) Shi, Y.; Li, H.; Li, L.-J. Recent Advances in Controlled Synthesis of Two-Dimensional Transition Metal Dichalcogenides via Vapour Deposition Techniques. *Chem. Soc. Rev.* **2015**, *44*, 2744−2756.

(8) Wang, Q. H.; Kalantar-Zadeh, K.; Kis, A.; Coleman, J. N.; Strano, M. S. Electronics and Optoelectronics of Two-Dimensional Transition Metal Dichalcogenides. *Nat. Nanotechnol.* **2012**, *7*, 699−712.

(9) Peng, X.; Peng, L.; Wu, C.; Xie, Y. Two Dimensional Nanomaterials for Flexible Supercapacitors. *Chem. Soc. Rev.* **2014**, *43*, 3303−3323.

(10) Bollella, P.; Fusco, G.; Tortolini, C.; Sanzò, G.; Favero, G.; Gorton, L.; Antiochia, R. Beyond Graphene: Electrochemical Sensors and Biosensors for Biomarkers Detection. *Biosens. Bioelectron.* **2017**, *89*, 152−166.

(11) Lv, R.; Robinson, J. A.; Schaak, R. E.; Sun, D.; Sun, Y.; Mallouk, T. E.; Terrones, M. Transition Metal Dichalcogenides and Beyond: Synthesis, Properties, and Applications of Single- and Few-Layer Nanosheets. *Acc. Chem. Res.* **2015**, *48*, 56−64.

(12) Spear, J. C.; Ewers, B. W.; Batteas, J. D. 2D-Nanomaterials for Controlling Friction and Wear at Interfaces. *Nano Today* **2015**, *10*, 301−314.

(13) Chia, X.; Eng, A. Y. S.; Ambrosi, A.; Tan, S. M.; Pumera, M. Electrochemistry of Nanostructured Layered Transition-Metal Dichalcogenides. *Chem. Rev.* **2015**, *115*, 11941−11966.

(14) Pumera, M.; Loo, A. H. Layered Transition-Metal Dichalcogenides (MoS_2 and WS_2) for Sensing and Biosensing. *TrAC, Trends Anal. Chem.* **2014**, *61*, 49−53.

(15) Teo, W. Z.; Chng, E. L. K.; Sofer, Z.; Pumera, M. Cytotoxicity of Exfoliated Transition-Metal Dichalcogenides (MoS_2, WS_2, and WSe_2) is Lower Than That of Graphene and its Analogues. *Chem. - Eur. J.* **2014**, *20*, 9627−9632.

(16) Newman, J. D.; Turner, A. P. Home Blood Glucose Biosensors: A Commercial Perspective. *Biosens. Bioelectron.* **2005**, *20*, 2435−2453.

(17) Gorodetskaya, I. A.; Gorodetsky, A. A. Analytical chemistry: Clamping Down on Cancer Detection. *Nat. Chem.* **2015**, *7*, 541−542.

(18) Wang, L.; Xiong, Q.; Xiao, F.; Duan, H. 2D Nanomaterials Based Electrochemical Biosensors for Cancer Diagnosis. *Biosens. Bioelectron.* **2017**, *89*, 136−151.

(19) Bhimanapati, G. R.; Lin, Z.; Meunier, V.; Jung, Y.; Cha, J.; Das, S.; Xiao, D.; Son, Y.; Strano, M. S.; Cooper, V. R.; Liang, L.; Louie, S. G.; Ringe, E.; Zhou, W.; Kim, S. S.; Naik, R. R.; Sumpter, B. G.; Terrones, H.; Xia, F.; Wang, Y.; Zhu, J.; Akinwande, D.; Alem, N.; Schuller, J. A.; Schaak, R. E.; Terrones, M.; Robinson, J. A. Recent Advances in Two-Dimensional Materials beyond Graphene. *ACS Nano* **2015**, *9*, 11509−11539.

(20) Eda, G.; Fujita, T.; Yamaguchi, H.; Voiry, D.; Chen, M.; Chhowalla, M. Coherent Atomic and Electronic Heterostructures of Single-Layer MoS_2. *ACS Nano* **2012**, *6*, 7311−7317.

(21) Py, M. A.; Haering, R. R. Structural Destabilization Induced by Lithium Intercalation in MoS_2 and Related Compounds. *Can. J. Phys.* **1983**, *61*, 76−84.

DOI: 10.1021/acsami.7b13090
ACS Appl. Mater. Interfaces 2017, 9, 40697−40706

(22) Papageorgopoulos, C. A.; Jaegermann, W. Li Intercalation across and along the van der Waals Surfaces of MoS_2 (0001). *Surf. Sci.* **1995**, *338*, 83−93.
(23) Chhowalla, M.; Shin, H. S.; Eda, G.; Li, L.-J.; Loh, K. P.; Zhang, H. The Chemistry of Two-Dimensional Layered Transition Metal Dichalcogenide Nanosheets. *Nat. Chem.* **2013**, *5*, 263−275.
(24) He, Z.; Que, W. Molybdenum Disulfide Nanomaterials: Structures, Properties, Synthesis and Recent Progress on Hydrogen Evolution Reaction. *Appl. Mater. Today* **2016**, *3*, 23−56.
(25) Vishnoi, P.; Sampath, A.; Waghmare, U. V.; Rao, C. N. R. Covalent Functionalization of Nanosheets of MoS_2 and $MoSe_2$ by Substituted Benzenes and Other Organic Molecules. *Chem. - Eur. J.* **2017**, *23*, 886−895.
(26) Manjunatha, S.; Rajesh, S.; Vishnoi, P.; Rao, C. N. R. Reaction with Organic Halides as A General Method for The Covalent Functionalization of Nanosheets of 2D Chalcogenides and Related Materials. *J. Mater. Res.* **2017**, *32*, 2984−2992.
(27) Lukowski, M. A.; Daniel, A. S.; Meng, F.; Forticaux, A.; Li, L.; Jin, S. Enhanced Hydrogen Evolution Catalysis from Chemically Exfoliated Metallic MoS_2 Nanosheets. *J. Am. Chem. Soc.* **2013**, *135*, 10274−10277.
(28) Voiry, D.; Salehi, M.; Silva, R.; Fujita, T.; Chen, M.; Asefa, T.; Shenoy, V. B.; Eda, G.; Chhowalla, M. Conducting MoS_2 Nanosheets as Catalysts for Hydrogen Evolution Reaction. *Nano Lett.* **2013**, *13*, 6222−6227.
(29) Chang, K.; Hai, X.; Pang, H.; Zhang, H.; Shi, L.; Liu, G.; Liu, H.; Zhao, G.; Li, M.; Ye, J. Targeted Synthesis of 2H- and 1T-Phase MoS_2 Monolayers for Catalytic Hydrogen Evolution. *Adv. Mater.* **2016**, *28*, 10033−10041.
(30) Liang, K. S.; Chianelli, R. R.; Chien, F. Z.; Moss, S. C. Structure of Poorly Crystalline MoS_2 — A Modeling Study. *J. Non-Cryst. Solids* **1986**, *79*, 251−273.
(31) Shi, Y.; Hua, C.; Li, B.; Fang, X.; Yao, C.; Zhang, Y.; Hu, Y.-S.; Wang, Z.; Chen, L.; Zhao, D.; Stucky, G. D. Highly Ordered Mesoporous Crystalline $MoSe_2$ Material with Efficient Visible-Light-Driven Photocatalytic Activity and Enhanced Lithium Storage Performance. *Adv. Funct. Mater.* **2013**, *23*, 1832−1838.
(32) Zhang, Y.; Zuo, L.; Zhang, L.; Huang, Y.; Lu, H.; Fan, W.; Liu, T. Cotton Wool Derived Carbon Fiber Aerogel Supported Few-Layered $MoSe_2$ Nanosheets as Efficient Electrocatalysts for Hydrogen Evolution. *ACS Appl. Mater. Interfaces* **2016**, *8*, 7077−7085.
(33) Chen, P.; Mccreery, R. L. Control of Electron Transfer Kinetics at Glassy Carbon Electrodes by Specific Surface Modification. *Anal. Chem.* **1996**, *68*, 3958−3965.
(34) Nicholson, R. S. Theory and Application of Cyclic Voltammetry for Measurement of Electrode Reaction Kinetics. *Anal. Chem.* **1965**, *37*, 1351−1355.
(35) Toh, R. J.; Mayorga-Martinez, C. C.; Han, J.; Sofer, Z.; Pumera, M. Group 6 Layered Transition-Metal Dichalcogenides in Lab-on-a-Chip Devices: 1T-Phase WS_2 for Microfluidics Non-Enzymatic Detection of Hydrogen Peroxide. *Anal. Chem.* **2017**, *89*, 4978−4985.
(36) Mayorga-Martinez, C. C.; Ambrosi, A.; Eng, A. Y. S.; Sofer, Z.; Pumera, M. Transition Metal Dichalcogenides (MoS_2, $MoSe_2$, WS_2 and WSe_2) Exfoliation Technique Has Strong Influence Upon Their Capacitance. *Electrochem. Commun.* **2015**, *56*, 24−28.
(37) Voiry, D.; Mohite, A.; Chhowalla, M. Phase Engineering of Transition Metal Dichalcogenides. *Chem. Soc. Rev.* **2015**, *44*, 2702−2712.
(38) Tsai, H.-L.; Heising, J.; Schindler, J. L.; Kannewurf, C. R.; Kanatzidis, M. G. Exfoliated−Restacked Phase of WS_2. *Chem. Mater.* **1997**, *9*, 879−882.
(39) Voiry, D.; Yamaguchi, H.; Li, J.; Silva, R.; Alves, D. C. B.; Fujita, T.; Chen, M.; Asefa, T.; Shenoy, V. B.; Eda, G.; Chhowalla, M. Enhanced Catalytic Activity in Strained Chemically Exfoliated WS_2 Nanosheets for Hydrogen Evolution. *Nat. Mater.* **2013**, *12*, 850−855.
(40) Heller, A.; Feldman, B. Electrochemical Glucose Sensors and Their Applications in Diabetes Management. *Chem. Rev.* **2008**, *108*, 2482−2505.
(41) Hecht, H. J.; Kalisz, H. M.; Hendle, J.; Schmid, R. D.; Schomburg, D. Crystal Structure of Glucose Oxidase from *Aspergillus niger* Refined at 2·3 Å Reslution. *J. Mol. Biol.* **1993**, *229*, 153−172.
(42) Bourdillon, C.; Demaille, C.; Moiroux, J.; Saveant, J.-M. Catalysis and Mass Transport in Spatially Ordered Enzyme Assemblies on Electrodes. *J. Am. Chem. Soc.* **1995**, *117*, 11499−11506.
(43) Bourdillon, C.; Demaille, C.; Moiroux, J.; Saveant, J.-M. Catalysis and Mass Transport in Spatially Ordered Enzyme Assemblies on Electrodes. *J. Am. Chem. Soc.* **1995**, *117*, 11499−11506.
(44) Long, G. L.; Winefordner, J. D. Limit of Detection. A Closer Look at the IUPAC Definition. *Anal. Chem.* **1983**, *55*, 712A−724A.
(45) Anto Jeffery, A.; Nethravathi, C.; Rajamathi, M. Two-Dimensional Nanosheets and Layered Hybrids of MoS_2 and WS_2 through Exfoliation of Ammoniated MS_2 (M = Mo,W). *J. Phys. Chem. C* **2014**, *118*, 1386−1396.
(46) Ambrosi, A.; Sofer, Z.; Pumera, M. 2H → 1T Phase Transition and Hydrogen Evolution Activity of MoS_2, $MoSe_2$, WS_2 and WSe_2 Strongly Depends on the MX_2 Composition. *Chem. Commun.* **2015**, *51*, 8450−8453.
(47) Human Serum H4522. http://www.sigmaaldrich.com/catalog/product/sigma/h4522?lang=en&ion=SG.
(48) Wu, S.; Zeng, Z.; He, Q.; Wang, Z.; Wang, S. J.; Du, Y.; Yin, Z.; Sun, X.; Chen, W.; Zhang, H. Electrochemically Reduced Single-Layer MoS_2 Nanosheets: Characterization, Properties, and Sensing Applications. *Small* **2012**, *8*, 2264−2270.
(49) Su, S.; Sun, H.; Xu, F.; Yuwen, L.; Fan, C.; Wang, L. Direct Electrochemistry of Glucose Oxidase and a Biosensor for Glucose Based on a Glass Carbon Electrode Modified with MoS_2 Nanosheets Decorated with Gold Nanoparticles. *Microchim. Acta* **2014**, *181*, 1497−1503.
(50) Parlak, O.; Incel, A.; Uzun, L.; Turner, A. P.; Tiwari, A. Structuring Au Nanoparticles on Two-Dimensional MoS_2 Nanosheets for Electrochemical Glucose Biosensors. *Biosens. Bioelectron.* **2017**, *89*, 545−550.
(51) Ambrosi, A.; Sofer, Z.; Pumera, M. Molybdenum Disulfide: Lithium Intercalation Compound Dramatically Influences the Electrochemical Properties of Exfoliated MoS_2. *Small* **2015**, *11*, 605−612.
(52) Toh, R. J.; Mayorga-Martinez, C. C.; Sofer, Z.; Pumera, M. 1T-Phase WS_2 Protein-Based Biosensor. *Adv. Funct. Mater.* **2017**, *27*, No. 1604923.

DOI: 10.1021/acsami.7b13090
ACS Appl. Mater. Interfaces 2017, 9, 40697−40706